Inorganic Chemistry

Article

pubs.acs.org/IC

Self-Assembly of Pentanuclear Mesocate versus Octanuclear Helicate: Size Effect of the $[M^{II}_3(\mu_3\text{-O/X})]^{n+}$ Triangle Core

Xin Bao,[†] Wei Liu,[†] Jun-Liang Liu,[†] Silvia Gómez-Coca,[‡] Eliseo Ruiz,*[,‡] and Ming-Liang Tong*[,†]

[†]Key Laboratory of Bioinorganic and Synthetic Chemistry of Ministry of Education, State Key Laboratory of Optoelectronic Materials and Technologies, School of Chemistry and Chemical Engineering, Sun Yat-Sen University, Guangzhou 510275, People's Republic of China

[‡]Departament de Química Inorgànica and Institut de Recerca de Química Teòrica i Computacional, Universitat de Barcelona, Diagonal 645, E-08028 Barcelona, Spain

Supporting Information

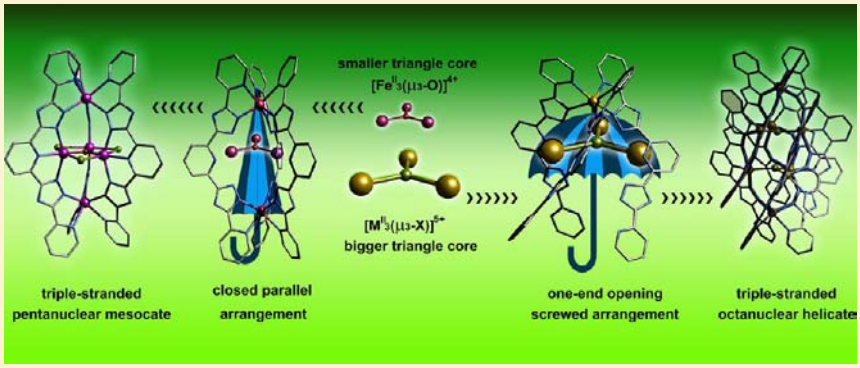

ABSTRACT: The first cluster mesocate $(H_3O)[\{Fe_2(\mu\text{-L})_3\}\{Fe_3(\mu_3\text{-O})(\mu\text{-Cl})_3\}]\cdot 3EtOH$ (**1**) and a new series of cluster helicates, $[\{Mn(\mu\text{-L})_3\}_2\{Mn_3(\mu_3\text{-Cl})\}_2](ClO_4)_2\cdot 2MeOH\cdot 6H_2O$ (**2**), $[\{Cd(\mu\text{-L})_3\}_2\{Cd_3(\mu_3\text{-Br})\}_2]Br_2\cdot 2DMF\cdot 14H_2O$ (**3**), and $[\{Cd(\mu\text{-L})_3\}_2\{Cd_3(\mu_3\text{-I})\}_2](CdI_4)\cdot 3H_2O$ (**4**), have been synthesized by the self-assembly of a C_2-symmetric tritopic ligand, 2,6-bis[5-(2-pyridinyl)-1*H*-triazol-3-yl]pyridine (H_2L) with different metal halogen salts. Single-crystal X-ray diffraction and electrospray ionization mass spectrometry measurements were carried out on these complexes. **1** was crystallized as a triple-stranded pentanuclear mesocate in which a $[Fe^{II}_3(\mu_3\text{-O})]^{4+}$ triangle core was wrapped by a $[Fe^{II}_2(\mu\text{-L})_3]^{2-}$ shell. **2**–**4** have similar octanuclear helicate structures in which two propeller-shaped $[M^{II}(\mu\text{-L})_3]^{4-}$ units embrace two $[M^{II}_3(\mu_3\text{-X})]^{5+}$ triangles inside. The $[M^{II}_3(\mu_3\text{-O/X})]^{n+}$ triangle core were found to play an important role in the selective synthesis of the two architectures: the smaller $[Fe^{II}_3(\mu_3\text{-O})]^{4+}$ triangle core prefers a mesocate structure because it matches the small cavity imposed by the $[Fe^{II}_2(\mu\text{-L})_3]^{2-}$ shell, while the bigger $[M^{II}_3(\mu_3\text{-X})]^{5+}$ induces a screwed arrangement of the ligands, thus stabilizing the helicate structure. Variable-temperature magnetic susceptibility measurements indicate that both **1** and **2** display an overall antiferromagnetic coupling. Density functional theory calculations for **1** confirm the strong antiferromagnetic interaction in the central $[Fe^{II}_3(\mu_3\text{-O})]^{4+}$, while interaction through the triazole bridging ligands is slightly ferromagnetic. For **2**, three interaction pathways were considered and all sets of J values reveal the presence of weak antiferromagnetic interaction.

INTRODUCTION

The self-assembly of polymetallic helicates has become one of the most fascinating topics of supramolecular chemistry in recent years.[1−8] The spontaneous formation of such organized architectures helps chemists to gain fundamental principles of recognition and self-assembly processes, which is helpful in the design of novel materials with programmed properties and functions.[9−16]

Many double- and triple-stranded linear helicates have been prepared by making use of coordination interactions between C_2-symmetric multi-bidentate ligands and four- or six-coordinated metal ions.[9−13] The metal centers in those complexes are chiral centers, being wrapped by two or three chelating ligands in a pseudotetrahedral or octahedral fashion and generating a two- or three-fold axis. Two possible architectures can be obtained according to the coupling of the chiral centers: homochiral helicates with ΔΔ or ΛΛ configuration and achiral mesocates with ΔΛ configuration. In most cases, racemic mixtures of helicates are the preferred products, while the formation of mesocates is far less common.[17−25] A great deal of effort has been dedicated to controlling the formation of helicates versus mesocates. Albrecht and Kotila found that the length of an alkyl spacer between two chelating moieties plays an important role in the diastereoselectivity. An empirical odd−even rule was proposed in which ligands with an even number of alkyl linkers prefer to stabilize a helicate while those with an odd number of alkyl linkers facilitate

Received: November 4, 2012
Published: December 27, 2012

   dx.doi.org/10.1021/ic3024056 | *Inorg. Chem.* 2013, 52, 1099−1107

the separation of a mesocate.[17] Enemark and Stack reported that engrafting *R*- and *S*-chiral groups in proximity to the chelating units allows the formation of diasteromerically and enantiomerically pure helicates.[18]

In most of these linear helicates, the metal centers are isolated and lack interaction. Developing a "cluster helicate" would rise above the limitation and improve the performance of helicates benefiting from the novel magnetic, electrical, and optical properties of metal clusters.[26] However, quite limited examples of cluster helicates have been reported because of the lack of an efficient synthetic strategy.[27−39] Bermejo et al. have successfully synthesized a series of tetranuclear helicates by using a dianionic helicand ligand equipped with two soft donor atoms in combination with metal(I) ions.[27,28] Another strategy is to introduce a $[M^{II}_3(\mu_3\text{-}O)]^{4+}$ triangle core into the helicates. A series of triple-stranded helicates with a $[M^{II}_3(\mu_3\text{-}O)]^{4+}$ core wrapped by terminal $[M^{II}(\mu\text{-}L)_3]^{n-}$ units have been synthesized and well-studied,[33−39] including our previously reported Fe_5 pentanuclear helicate.[39]

Encouraged by the fascinating architecture and intriguing properties of the Fe_5 cluster based on the bitopic 3,5-bis(pyridin-2-yl)-1,2,4-triazole ligand,[39] we expected that a related C_2-symmetric, tritopic ligand, 2,6-bis[5-(2-pyridinyl)-1*H*-triazol-3-yl]pyridine (H_2L), could possibly afford an intriguing triple-stranded structure of higher nuclearity. In contrast to the long and flexible bidentate−tridentate−bidentate segmental ligands being exploited by Piguet et al. to construct d−f−d trinuclear helicates,[40−42] the relatively short and rigid H_2L ligand in our case may not afford an appropriate coordination environment for a single metal ion in the central position but may be suitable for incorporating a bigger metal cluster alternatively, probably a $[M^{II}_3(\mu_3\text{-}O)]^{4+}$ triangle core. Indeed, via the solvothermal reaction of the H_2L ligand with different halide salts, we have successfully synthesized the first cluster mesocate $(H_3O)[\{Fe_2(\mu\text{-}L)_3\}\{Fe_3(\mu_3\text{-}O)(\mu\text{-}Cl)_3\}]\cdot 3EtOH$ (**1**) and a new series of octanuclear helicates: $[\{Mn(\mu\text{-}L)_3\}_2\{Mn_3(\mu_3\text{-}Cl)\}_2](ClO_4)_2\cdot 2MeOH\cdot 6H_2O$ (**2**), $[\{Cd(\mu\text{-}L)_3\}_2\{Cd_3(\mu_3\text{-}Br)\}_2]Br_2\cdot 2DMF\cdot 14H_2O$ (**3**), and $[\{Cd(\mu\text{-}L)_3\}_2\{Cd_3(\mu_3\text{-}I)\}_2](CdI_4)\cdot 3H_2O$ (**4**). It should be noted that in these helicate structures, **2**−**4**, a bigger halogen atom takes the central position instead of the O atom. Our results show that the $[M_3(\mu_3\text{-}O/X)]$ triangle core not only plays a crucial role in the formation of triple-stranded structures but also serves to discriminate mesocate and helicate through the size effect (Scheme 1).

Scheme 1

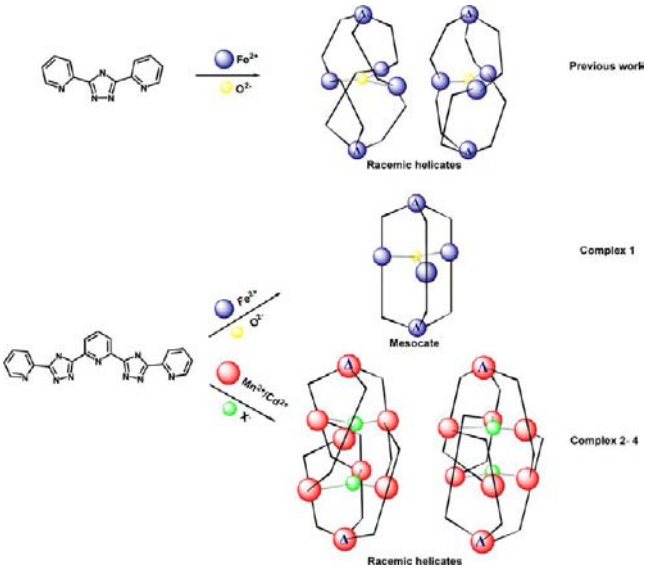

EXPERIMENTAL SECTION

Materials and General Procedures. All of the chemicals were obtained from commercial sources and used without further purification. The IR spectra were recorded from KBr disks in the range 4000−400 cm^{-1} with a Bruker tensor 27 spectrometer. The C, H, and N elemental analyses of the crystal samples were performed on an Elementar Vario EL elemental analyzer. Electrospray ionization mass spectrometry (ESI-MS) spectra were recorded on a Thermo-Finnigan LCQ DECA XP quadrupole ion-trap mass spectrometer using an electrospray ionization source. Data were processed using the spectrometer software (*MassLynx NT*, version 3.4). Because of the poor solubility of all of the complexes, dimethylformamide (DMF)-containing crystal samples were sonicated vigorously and then filtered before ESI-MS measurements were carried out. Temperature-dependent magnetic susceptibility data for polycrystalline complexes of **1** and **2** were performed using a Quantum Design MPMS-XL-7 SQUID magnetometer under an applied field of 500 Oe over the temperature range of 2−300 K. The samples were packed into plastic films, which were then mounted in low-background diamagnetic plastic straws. The data were corrected for diamagnetism of the constituent atoms using Pascal constants and magnetization of the sample holder.

Synthesis of Complexes 1−4. *$[\{Fe_2(\mu\text{-}L)_3\}\{Fe_3(\mu_3\text{-}O)(\mu\text{-}Cl)_3\}](H_3O)(EtOH)_3$ (**1**).* An ethanol (10 mL) solution of $FeCl_2\cdot 4H_2O$ (0.034 g, 0.17 mmol), 2,6-bis[5-(2-pyridinyl)-1*H*-triazol-3-yl]pyridine (H_2L; 0.037 g, 0.1 mmol), and triethylamine (0.010 g, 0.1 mmol) was sealed in a 15 mL Teflon-lined reactor, heated at 160 °C for 3 days, and then cooled to room temperature at 5 °C h^{-1}. Subsequently, hexagonal-prism dark-red crystals were obtained in 10% yield based on Fe. IR (KBr, cm^{-1}): 3422 br s, 1607 s, 1580 s, 1503 s, 1459 s, 1406 s, 1338 w, 1282 w, 1254 w, 1192 m, 1125 m, 1051 m, 1007 m, 812 m, 752 s, 670 s. Elem anal. Calcd (%): C, 45.72; H, 3.29; N, 22.85. Found: C, 45.68; H, 3.02; N, 22.51.

*$[\{Mn(\mu\text{-}L)_3\}_2\{Mn_3(\mu_3\text{-}Cl)\}_2](ClO_4)_2\cdot 2MeOH\cdot 6H_2O$ (**2**).* A methanol (10 mL) solution of $MnCl_2\cdot 4H_2O$ (0.026 g, 0.13 mmol), $NaClO_4$ (0.004 g, 0,033 mmol), H_2L (0.037 g, 0.1 mmol), and triethylamine (0.010 g, 0.1 mmol) was sealed in a 15 mL Teflon-lined reactor, heated at 160 °C for 3 days, and then cooled to room temperature at 5 °C h^{-1}. Subsequently, blocky colorless crystals were obtained in 60% yield based on Mn. IR (KBr, cm^{-1}): 3419 br s, 1605 s, 1573 s, 1504 s, 1461 s, 1431 m, 1407 s, 1338 w, 1289 w, 1279 w, 1191 m, 1120 br s, 1047 m, 1017 m, 823 m, 806 m, 749 s, 729 s. Elem anal. Calcd: C, 45.33; H, 2.82; N, 24.61. Found: C, 45.28; H, 3.15; N, 24.50.

*$[\{Cd(\mu\text{-}L)_3\}_2\{Cd_3(\mu_3\text{-}Br)\}_2]Br_2\cdot 2DMF\cdot 14H_2O$ (**3**).* An ethanol/DMF (6/4 mL) solution of $CdBr_2\cdot 4H_2O$ (0.045 g, 0.13 mmol), H_2L (0.037 g, 0.1 mmol), and triethylamine (0.010 g, 0.1 mmol) was sealed in a 15 mL Teflon-lined reactor, heated at 160 °C for 3 days, and then cooled to room temperature at 5 °C h^{-1}. Subsequently, colorless crystals were obtained in 54% yield based on Cd. IR (KBr, cm^{-1}): 3426 br s, 1603 s, 1573 s, 1499 s, 1459 m, 1407 s, 1338 w, 1289 w, 1278 w, 1189 m, 1150 w, 1049 w, 1013 w, 803 m, 748 m, 728 m. Elem anal. Calcd: C, 39.49; H, 2.98; N, 21.49. Found: C, 38.82; H, 2.87; N, 20.50.

*$[\{Cd(\mu\text{-}L)_3\}_2\{Cd_3(\mu_3\text{-}I)\}_2](CdI_4)\cdot 3H_2O$ (**4**).* A methanol (10 mL) solution of $CdI_2\cdot 4H_2O$ (0.047 g, 0.13 mmol), H_2L (0.037 g, 0.1 mmol), and triethylamine (0.010 g, 0.1 mmol) was sealed in a 15 mL Teflon-lined reactor, heated at 160 °C for 3 days, and then cooled to room temperature at 5 °C h^{-1}. Subsequently, hexagonal-prism colorless crystals were obtained in 55% yield based on Cd. IR (KBr, cm^{-1}): 3428 br s, 1603 s, 1573 s, 1499 m, 1459 w, 1406 s, 1338 w, 1278 w, 1189 w, 1150 w, 1049 w, 1013 w, 802 m, 748 m, 728 m. Elem anal. Calcd: C, 34.07; H, 1.81; N, 18.82. Found: C, 34.13; H, 2.10; N, 18.91.

X-ray Crystallography. The intensity data were collected on a Rigaku R-Axis Spider IP diffractometer (Mo Kα, λ = 0.71073 Å) for **1**, on an Oxford Diffraction Gemini R CCD diffractometer with Cu Kα radiation (λ = 1.54178 Å) for **2** and **3**, or on a Bruker SMART Apex CCD diffractometer with Cu Kα radiation (λ = 1.54178 Å) for **4**. CCDC 883876, 883878, 883879, and 883880 contain the supplementary crystallographic data for this paper. These data can be obtained free of charge from The Cambridge Crystallographic Data Centre via www.ccdc.cam.ac.uk/data_request/cif.

dx.doi.org/10.1021/ic3024056 | *Inorg. Chem.* 2013, 52, 1099−1107

Table 1. Crystallographic Data and Structural Refinement Summary for 1−4

	1	2	3	4
formula	$C_{63}H_{54}Cl_3Fe_5N_{27}O_5$	$C_{116}H_{86}Mn_8Cl_4N_{54}O_{16}$	$C_{120}H_{108}Cd_8Br_2N_{56}O_{16}$	$C_{114}H_{72}Cd_9I_6N_{54}O_3$
fw	1654.93	3073.7	3649.6	4019.26
temperature, K	298(2)	150(2)	150(2)	150(2)
cryst syst	hexagonal	monoclinic	monoclinic	trigonal
space group	$P6_3/m$	$C2/c$	$C2/c$	$P3c1$
a, Å	12.7902(5)	42.2021(11)	42.575(4)	13.8430(3)
b, Å	12.7902(5)	13.7700(1)	13.9018(4)	13.8430(3)
c, Å	22.4082(15)	24.8281(5)	25.2129(16)	41.0426(14)
α, deg	90	90	90	90
β, deg	90	122.843(3)	121.888(10)	90
γ, deg	120	90	90	120
V, Å^3	3174.6(3)	12122.0(4)	1132.81(7)	6811.2(3)
Z	2	4	4	2
$F(000)$	1684	6224	7488	3816
ρ_{calcd}, g cm^{-3}	1.731	1.684	1.997	1.960
μ(Mo Kα), mm^{-1}	1.319	8.132	12.773	22.265
θ range, deg	3.19−27.38	2.49−60.00	3.41−62.47	3.69−59.99
reflns collected, R_{int}	8151, 0.0670	11876, 0.0208	16188, 0.0361	13467, 0.0310
indep reflns	2447	5944	9780	4821
R1[a] [$I > 2\sigma(I)$]	0.0586	0.0518	0.0529	0.0385
wR2[b] (all data)	0.2110	0.1452	0.1314	0.108
GOF	1.127	1.041	1.099	1.076
Flack x parameter				0.00(3)

[a] $R1 = \sum||F_o| - |F_c||/\sum|F_o|$. [b] $wR2 = [\sum w(F_o^2 - F_c^2)^2/\sum w(F_o^2)^2]^{1/2}$.

The structures were solved by direct methods, and all non-H atoms were refined anisotropically by least squares on F^2 using the *SHELXTL* program. H atoms on organic ligands were generated by the riding model (Sheldrick, G. M. *SHELXTL97, Program for crystal structure refinement*; University of Göttingen: Göttingen, Germany, 1997). Electron density contributions from disordered water molecules were handled using the *SQUEEZE* procedure from the *PLATON* software (Spek, A. L. *J. Appl. Crystallogr.* **2003**, *36*, 7−13). A summary of the crystallographic data and refinement parameters is provided in Table 1.

RESULTS AND DISCUSSION

Syntheses and ESI-MS Studies. Single crystals of **1** consisting of pentanuclear mesocates were synthesized by a one-pot solvothermal reaction of $FeCl_2{\cdot}4H_2O$, H_2L, and triethylamine in a 5:6:6 molar ratio. When $FeCl_2{\cdot}4H_2O$ was changed into $MnCl_2{\cdot}4H_2O$, $CdBr_2{\cdot}4H_2O$, and $CdI_2{\cdot}4H_2O$, complexes **2**−**4** were obtained, respectively, and found to have octanuclear helicates. The molar ratio of metal salts and ligands as well as the solvents were adjusted subsequently to pursue a better yield for complexes **2**−**4**. The final conditions were described in the Experimental Section.

All of the samples are poorly soluble even after a vigorous ultrasonic oscillation treatment in a DMF solvent. ESI-MS measurements were still carried out for the filtrate. The spectra of complexes **2**−**4** are shown in Figures 1−3. The predominant peak with isotopic distributions of 0.5 peak separation allowed the unambiguous assignment of 2+-charged species $[Mn^{II}_8L_6Cl_2]^{2+}$ (m/z 1351.3), $[Cd^{II}_8L_6Br_2]^{2+}$ (m/z 1625.9), and $[Cd^{II}_8L_6I_2]^{2+}$ (m/z 1672.9), respectively, agreeing well with the formation of octanuclear cations confirmed by single-crystal measurements. Unfortunately, for complex **1**, it decomposed after the ultrasonic process and displayed numerous peaks in the ESI-MS spectrum (Figure S1 in the Supporting Information, SI). Nevertheless, among these peaks, the ones corresponding to $[Fe^{II}_5L_3OCl + nKCl]^+$ species were identified. As a further attempt, a DMF solvent containing crystals of **1** without oscillation was also prepared and left for several days before measurement. However, no related ion peak could be observed because of insolubility (Figure S2 in the SI).

Single-Crystal X-ray Structure of 1. Complex **1** crystallizes in the hexagonal space group $P6_3/m$. It consists of $[\{Fe_2(\mu\text{-}L)_3\}\{Fe_3(\mu_3\text{-}O)(\mu\text{-}Cl)_3\}]^-$ pentanuclear mesocates, H_3O^+ countercations, and EtOH solvent molecules. The structure of the mesocate is shown in Figure 4. Five Fe ions define a trigonal-bipyramidal polyhedron, in which the $Fe_{apical}{-}Fe_{equatorial}$, $Fe_{equatorial}{-}Fe_{equatorial}$, and $Fe_{apical}{-}Fe_{apical}$ distances are 3.2590(17), 4.7459(12), and 8.714(3) Å, respectively. Three C_2-symmetric ligands wrap the polyhedron along its vertical edges in a side-by-side style; each ligand coordinates to two apical and one equatorial ions using two bidentate sites at the ends and one tridentate site, respectively. Three equatorial Fe ions form an equilateral triangle assisted by a central μ_3-O-bridging atom and three peripheral μ-Cl ions. The O atom locates exactly in the center of the Fe_3 triangle, exhibiting a uniform Fe−O bond length of 1.8816(10) Å. Three Cl atoms are coplanar to the Fe3 triangle plane; they sit asymmetrically between two neighboring Fe ions, resulting in a longer Fe−Cl distance of 2.759(3) Å and a shorter one of 2.500(2) Å. Each equatorial Fe ion is in a distorted N_3OCl_2 octahedral geometry with $Fe{-}N_{pyridine}$ and $Fe{-}N_{triazole}$ bond lengths of 2.226(4) and 2.183(5) Å, respectively. Each apical ion also locates in a distorted octahedral environment, being coordinated by six N atoms from three chelating ligands, thus becoming a chiral center. The $Fe{-}N_{pyridine}$ and $Fe{-}N_{triazole}$ bond lengths are 2.355(4) and 2.184(4) Å, respectively. The bond lengths of these Fe ions are typical of Fe^{II} in the high-spin state. The mesocate molecule is of an ideal C_{3h} symmetry, possessing a C_3 rotation axis passing through the two apical Fe ions and the central μ_3-O atom as well as a orthogonal mirror plane defined by the $\{Fe_3(\mu_3\text{-}O)(\mu\text{-}Cl)_3\}$ triangle core. The two

dx.doi.org/10.1021/ic3024056 | *Inorg. Chem.* 2013, 52, 1099−1107

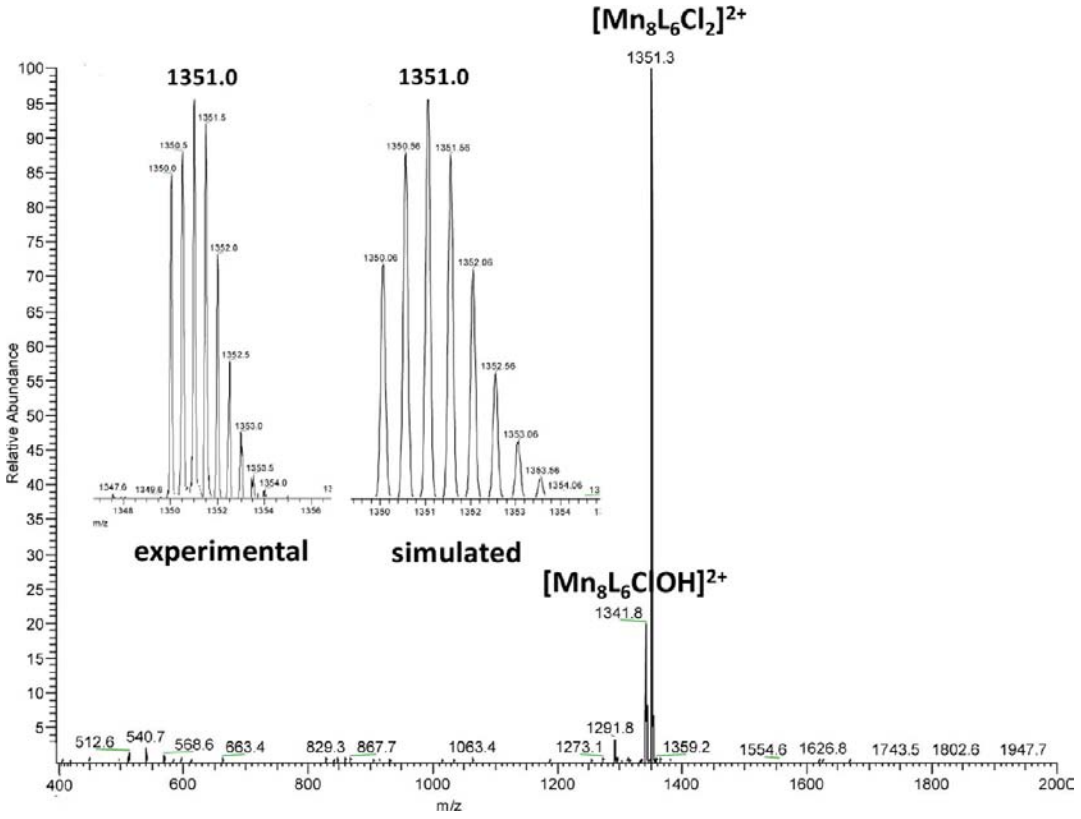

Figure 1. ESI-MS spectra of **2**. The insets show the experimental and simulated isotopic distributions of the species.

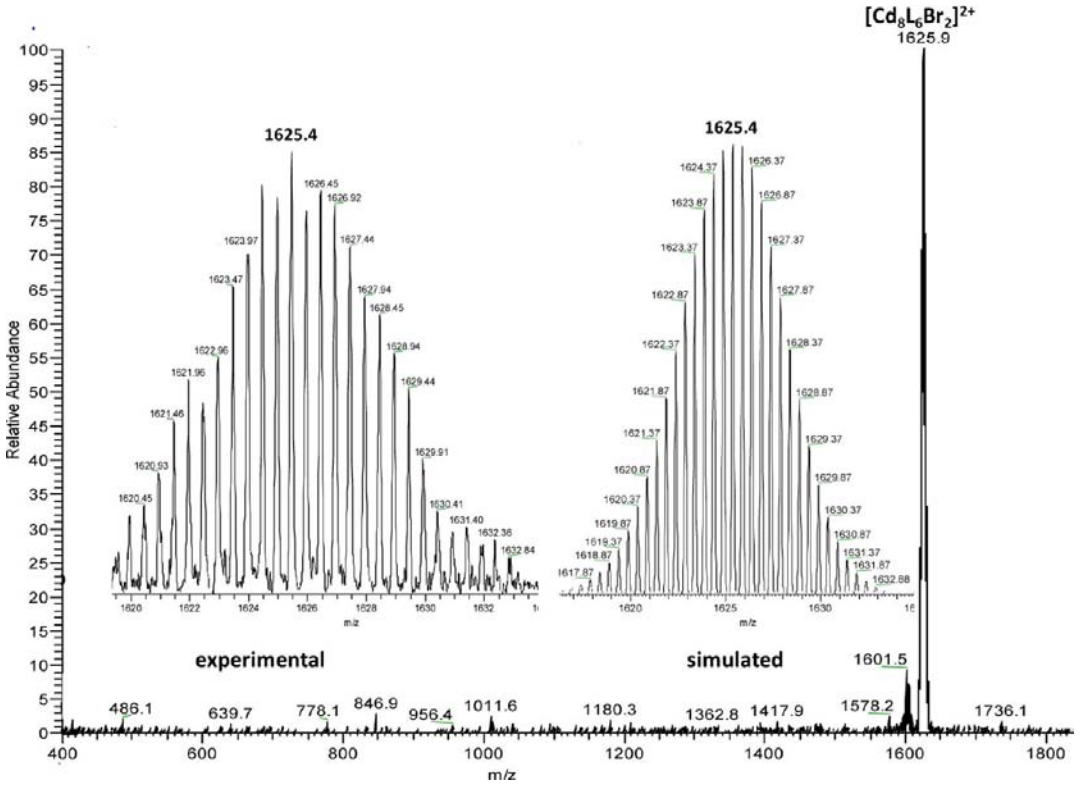

Figure 2. ESI-MS spectra of **3**. The insets show the experimental and simulated isotopic distributions of the species.

chiral apical Fe ions possess opposite chirality (Δ and Λ) because of the side-by-side (nonhelical) arrangement of the ligands, giving rise to a triple-stranded achiral mesocate.

Single-Crystal X-ray Structures of 2−4. Complexes **2**-**4** contain similar triple-stranded octanuclear cationic helicates but different counteranions and solvents.

dx.doi.org/10.1021/ic3024056 | *Inorg. Chem.* 2013, 52, 1099−1107

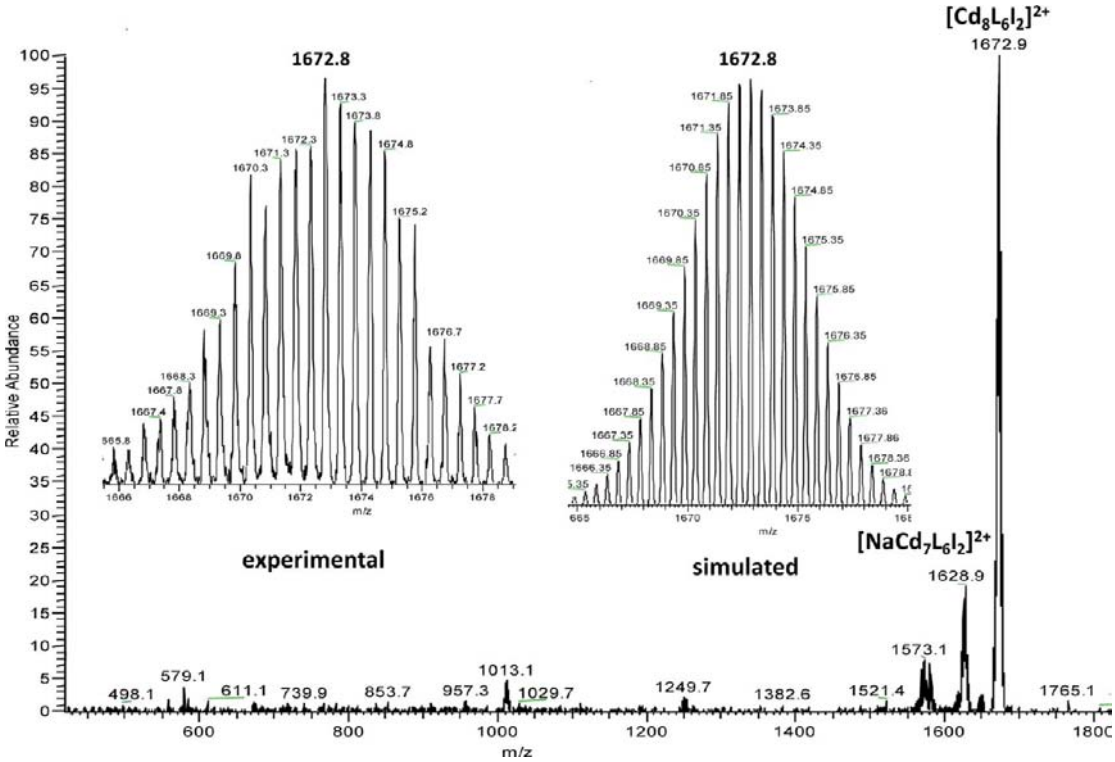

Figure 3. ESI-MS spectra of **4**. The insets show the experimental and simulated isotopic distributions of the species.

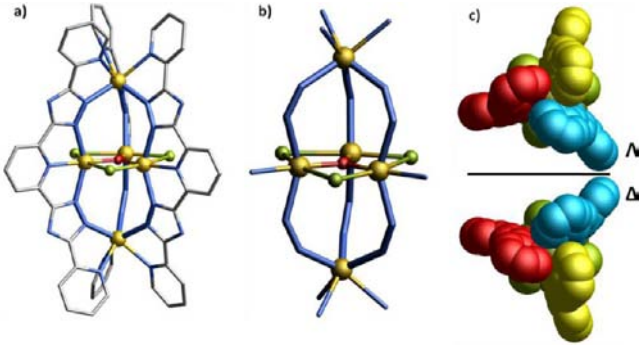

Figure 4. Structural features of the pentanuclear mesocate in complex **1**: (a) ball-and-stick representation of the mesocate; (b) coordination environments and bridging pathways of Fe ions; (c) view of the mesocate in space-filling mode from the *c* and *c** directions. Color code in parts a and b: Fe, yellow; C, gray; N, blue; O, red; Cl, green. H atoms are omitted for clarity.

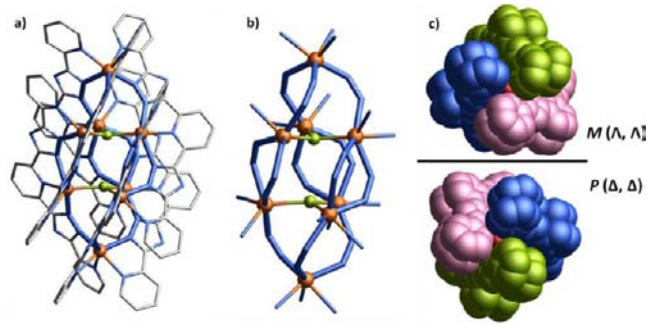

Figure 5. Structural features of the octanuclear helicate in complex **2**: a) Ball-and-stick representation of the ΔΔ-configurational helicate; b) the coordination environments and bridging pathways of Mn ions and c) Space-filling representation of the two enantiomers present in **2**. Color code in a) and b): Mn orange, C gray, N blue, O red,Cl green. H atoms are omitted for clarity.

Complex **2** crystallizes in the monoclinic space group *C*2/*c* and consists of $[\{Mn(\mu\text{-}L)_3\}_2\{M_3(\mu_3\text{-}Cl)\}_2]^{2+}$ cationic helicates, ClO_4^- anions, MeOH and H_2O solvent molecules. The structure of the helicate is shown in Figure 5a. Eight Mn ions form a distorted bicapped trigonal antiprism polyhedron, in which two offset Mn_3 triangles bridged by μ_3-Cl atoms define the antiprism, and the rest two Mn ions locate above and below the triangle faces. Only half of the Mn ions are independent as a two-fold rotation axis pass through the center. Average distance between an apical Mn ion and an ion in the adjacent triangle is 4.62 Å, and mean distance between two Mn^{II} ions of different Mn_3 triangles is 4.49 Å. Unlike the equivalent Fe_3 triangle in **1**, the Mn_3 triangle is scalene with an average Mn−Mn distance of 4.14 Å, which is in accordance with the lower symmetry. In addition, the Cl atom does not sit in the center of the triangle, it deviate slightly (0.31 Å) from the Mn_3 plane and bridges three Mn ions asymmetrically with an average Mn−Cl bond length of 2.41 Å. Three pairs of ligands with strong offset face-to-face $\pi-\pi$ stacking interactions (3.37−3.55 Å) wrap the Mn_8 polyhedron in a propeller-like form. The coordination environments of metal ions are shown in Figure 5b. Each Mn ion in the triangle is octahedrally coordinated by a Cl atom and five N atoms from two ligands. Mn−N bond lengths follow in the range of 2.18−2.50 Å. The apical Mn ion is wrapped by three ligands with their bidentate chelating sites and adopts distorted octahedral geometry. Average Mn−N bond length is 2.27 Å. In contrast to **1**, the two apical ions possess the same chirality due to a screwed arrangement of the ligands, resulting in a triple-stranded *M*(Λ, Λ) or *P*(Δ, Δ) helix. (Figure 5c) Homochiral helicates pack in *ab* planes via H-bond interactions with ClO_4^- anions and solvent molecules, giving rise to chiral layers. However, layers with opposite chirality stack alternatively through $\pi-\pi$ interactions along the *c* axis, resulting in the overall racemic complex (Figure 6).

dx.doi.org/10.1021/ic3024056 | *Inorg. Chem.* 2013, 52, 1099−1107

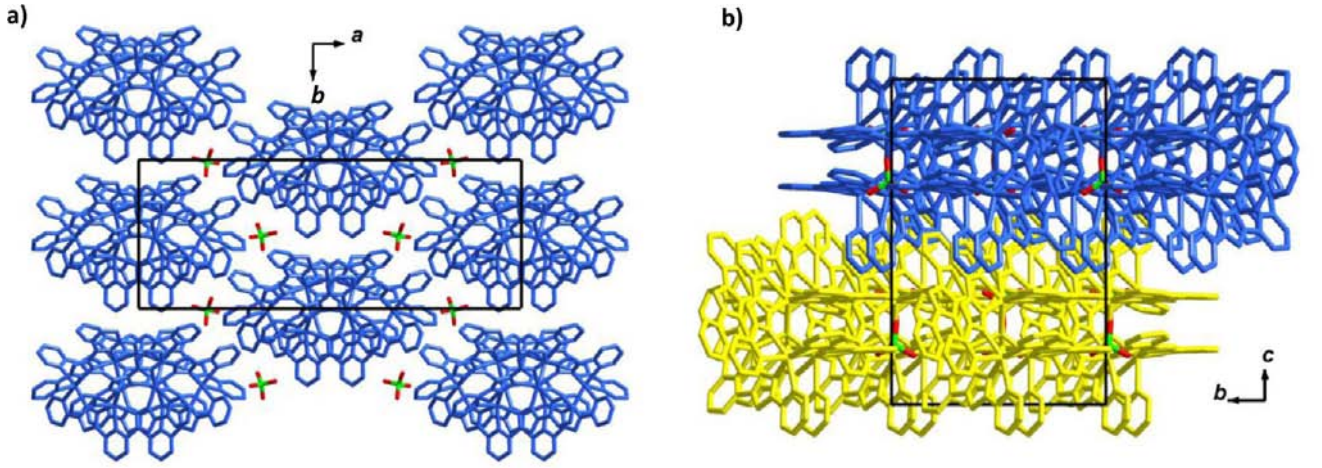

Figure 6. Packing diagram of **2** showing a homochiral layer packed in the *ab* plane (a) and heterochiral layers running along the *c* axis alternatively (b).

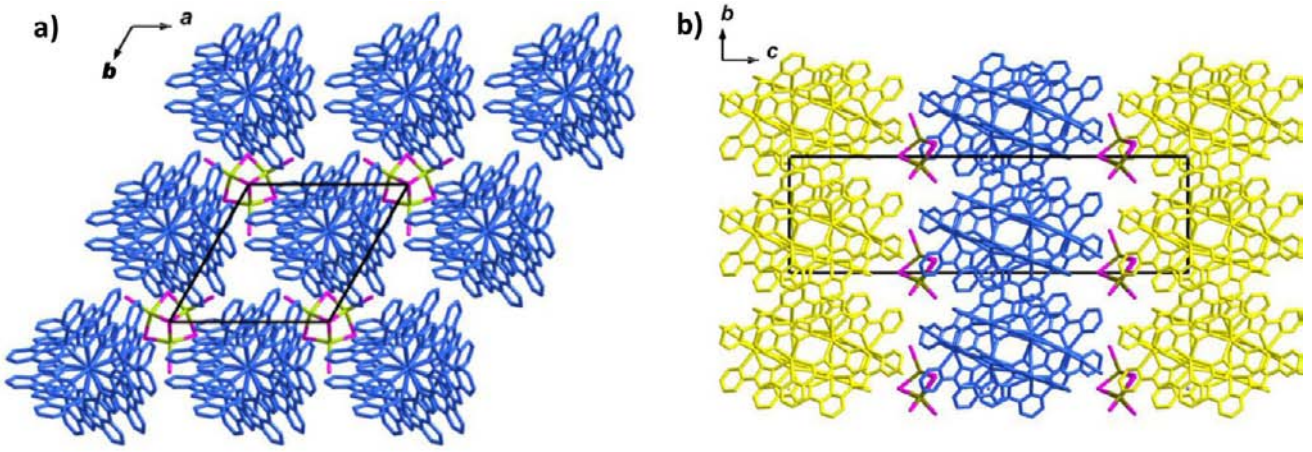

Figure 7. Packing diagram of **4** showing a homochiral layer packed in the *ab* plane (a) and heterochiral layers running along the *c* axis alternatively (b).

Complex **3** also crystallizes in space group $C2/c$. The structure of the helicate and the three-dimensional crystal packing are quite similar to those in **2**. However, due to the incorporation of bigger metal ions all coordination bond lengths elongate: Cd−N bond lengths follow in the range of 2.27−2.55 Å and Cd−Br bond lengths are between 2.65 and 2.73 Å. The size of the Cd_8 polyhedron expand as well, with Cd−Cd distances of 4.59 Å (Cd ions in different triangles), 4.67 Å (an apical and an equatorial Cd ion) and 4.67 Å (Cd ions in the same triangle), respectively. In addition, the intramolecular $\pi-\pi$ stacking interactions are weakened to 3.56−3.92 Å.

Complex **4** crystallizes in trigonal space group $P3c1$.[43] Although the helicate is of C_3 rather than C_2 symmetry, the overall arrangement is still quite similar to those in **2** and **3**. There is a three-fold rotation axis passing through the apical Cd ions and the central μ_3-Cl ions; as a result, the two Cd_3 triangles are equilateral with edge lengths of 4.9329(15) and 4.9253(15) Å, respectively. The Cd−N bond lengths follow in the range of 2.29−2.58 Å and are comparable with those in complex **3**; the Cd−I bond lengths in two triangles are 2.8464(9) and 2.8590(9) Å, respectively. As shown in Figure 7, the crystal packing in **4** is different from those in **2** and **3**; nevertheless, it still consists of homochiral layers stacking in the *ab* planes and heterochiral supramolecular layers running along the *c* axis alternatively.

Formation of Mesocate versus Helicate. The mesocate structure can be interpreted as a closed $[Fe^{II}_2(\mu\text{-}L)_3]^{2-}$ shell wrapping a $[Fe^{II}_3(\mu_3\text{-}O)]^{4+}$ triangle core inside, while the helicate structure can be viewed as two propeller-shaped $[M^{II}(\mu\text{-}L)_3]^{4-}$ units embedded together through $\pi-\pi$ interactions, wrapping two $[M^{II}_3(\mu_3\text{-}X)]^{5+}$ triangles inside. In view of the symmetry demand, a $[M^{II}_3(\mu_3\text{-}O/X)]^{n+}$ triangle core can provide a three-fold axis and a mirror plane for an idealized C_{3h}-symmetric triple-stranded mesocate as well as a two-fold axis along the $M^{II}-O/X$ bond for an idealized D_3-symmetric helicate, thus being utilized as the perfect template to assist the formation of such structures. Particularly in this case, the helicate and mesocate can be selectively stabilized by the triangles of different sizes; namely, the smaller $[Fe^{II}_3(\mu_3\text{-}O)]^{4+}$ triangle (triangle edge length = 3.2 Å) prefers the formation of a mesocate, while the bigger $[M^{II}_3(\mu_3\text{-}X)]^{5+}$ triangle ($[Mn_3(\mu_3\text{-}Cl)]^{5+}$ = 4.1 Å, $[Cd^{II}_3(\mu_3\text{-}Br)]^{5+}$ = 4.7 Å, and $[Cd^{II}_3(\mu_3\text{-}Br)]^{5+}$ = 4.9 Å) inclines to stabilize a helical product. Such selectivity arises from the size matching effect between the cavity formed by the $[Fe^{II}_2(\mu\text{-}L)_3]^{2-}$ or $[M^{II}(\mu\text{-}L)_3]_2^{8-}$ shell and the included triangle cores. In the mesocate family, three wrapping ligands adopt a "closed" arrangement, resulting in a small cavity whose size is restricted in order to ensure reasonable coordination geometries of the apical metal ions. As a result, only the smaller $[Fe^{II}_3(\mu_3\text{-}O)]^{4+}$ core matches the cage perfectly, while the others are too big to be embraced. In contrast, the cage in the helicate family is bigger and more adjustable because the two $[M^{II}(\mu\text{-}L)_3]^{4-}$ units adopt a screwed

dx.doi.org/10.1021/ic3024056 | *Inorg. Chem.* 2013, 52, 1099−1107

one-end-opening arrangement, allowing for the inclusion of a bigger triangle core.

It is worth mentioning that the yields of the helicate complexes **2**−**4** (>50%) are much higher than that of the mesocate complex **1** (<10%). Theoretically, homochiral helicates are the consistently preferred product in the self-assembly process because they have a lower total energy.[19] In the present case, the ligand in the mesocate is seriously distorted in order to satisfy the coordination environments of the metal ions as well as to avoid a crash between the three head pyridines around the apical ion (Figure S3 in the SI), while such a strain is effectively released in the helicate because of a flexible screwed coordination mode. Besides, the helicate structure could be additionally stabilized by abundant intamolecular $\pi-\pi$ stacking interactions. However, the mesocate structure could still be obtained because of kinetic trapping in the presence of the appropriate triangle core template and rapid separation benefiting from the low solubility.

Magnetic Properties. Magnetic susceptibility measurements were carried out on crystalline samples of **1** and **2** with an applied magnetic field of 500 Oe in the temperature range of 300−2 K. As shown in Figure 8, the $\chi_M T$ value of **1** is 12.3 cm^3 K mol^{-1} at 300 K,

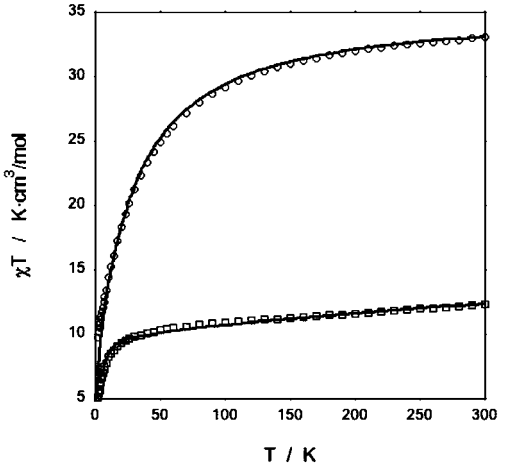

Figure 8. Variable-temperature magnetic susceptibility studies of **1** (□) and **2** (○). The solid lines correspond to the fitted J values collected in Table 2.

which is smaller than the spin-only value (15 cm^3 K mol^{-1}) for five noninteracting high-spin Fe^{II} ions (S = 2), assuming an isotropic g value of 2.00. Upon cooling, the $\chi_M T$ value gradually decreases to 10.3 cm^3 K mol^{-1} at 50 K and then drops sharply to 5.1 cm^3 K mol^{-1} at 2 K. The sharp decrease below 50 K is probably due to the zero-field-splitting effect. The $\chi_M T$ value of **2** at 300 K is 32.9 cm^3 K mol^{-1}, corresponding to eight isolated Mn^{II} ions ($S = {}^5/_2$; $g \approx 2$). With decreasing temperature, the $\chi_M T$ value decreases to 9.79 cm^3 K mol^{-1} at 2 K. The magnetic behavior of **1** and **2** suggests the existence of an overall antiferromagnetic coupling in these complexes.

Electronic structure calculations based on density functional theory (DFT) have been employed to obtain the exchange coupling constant values for **1** and **2**. The B3LYP function[44] and an all-electron basis set[45] using the *Jaguar*[46] and *Gaussian*[47] codes were employed following a procedure described previously,[48−52] using the following Heisenberg−Dirac−van Vleck Hamiltonian:

$$\hat{H} = -\sum_{a<b} J_{ab}\hat{S}_a\hat{S}_b \qquad (1)$$

where the J_{ab} values are the exchange coupling constants between the different paramagnetic centers present in the system. Two exchange coupling constants were adopted for the highly symmetric Fe_5 complex **1** (Figure 9a): the J_1 value between two

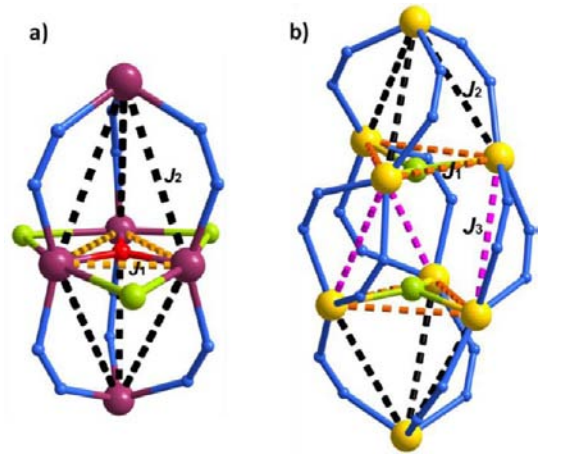

Figure 9. Magnetic exchange coupling pathways in **1** (a) and **2** (b).

Fe^{II} ions of the triangle and the J_2 value between a Fe^{II} ion in the triangle core and an axial Fe^{II} ion. In the case of the Mn_8 complex **2**, three J values were considered (Figure 9b): J_1 between two Mn^{II} ions of the same triangle, J_2 for the coupling of a Mn^{II} ion in the triangle and an apical Mn^{II} ion, and J_3 between two Mn^{II} ions of different Mn_3 triangles. A $[\{Fe^{II}{}_2(\mu\text{-L})_3\}\{Fe^{II}{}_3(\mu_3\text{-O})(\mu\text{-X})_3\}]^-$ model and a $[\{Mn^{II}(\mu\text{-L})_3\}_2\{Mn^{II}{}_3(\mu_3\text{-Cl})\}_2]^{2+}$ model were employed for **1** and **2**, respectively. The calculated values are collected in Table 1.

The results for **1** show a predominant antiferromagnetic interaction in the central Fe_3 triangle, while the interaction through the triazole bridging ligands is slightly ferromagnetic, leading to an $S = {}^5/_2$ ground sate. Using these calculated values as the starting set of a fitting procedure of the experimental magnetic susceptibility, similar fitted J values (see Table 2 and Figure 8)

Table 2. Calculated DFT J Values (in cm^{-1}) and Those Fitted Using Experimental Magnetic Susceptibility (See Figure 8) of 1 and 2

complex	J value	bridging ligand	J_{calc}	J_{fit}
1	J_1	(μ_3-O)(μ-Cl)	−52.3	−41.2
	J_2	(μ-N_2:triazole)	+4.0	+7.6
2	J_1	(μ_3-Cl)	−9.1	−2.6
	J_2	(μ-N_2:triazole)	−0.4	−0.2
	J_3	2(μ-N_2:triazole)	−1.1	−0.7

were obtained with a g value of 2.04. Although there is no precedent $\{Fe^{II}{}_3(\mu\text{-Cl})_3(\mu_3\text{-O})\}^+$ unit in the literature to compare with, the case for both metal ions bearing one unpaired electron in the $d_{x^2-y^2}$ orbital promotes a relatively strong antiferromagnetic interaction in the presence of chloride and oxo bridging ligands, thus providing a good overlap between such magnetic orbitals.

For comparison, DFT calculations were also carried out for our previously reported similar Fe_5 complex,[39] which has an inequilateral Fe_3 triangle bridged by a μ_3-O center and adopts a less symmetric structure. The calculated B3LYP average J_1 and J_2 values are −64.7 and −0.85 cm^{-1}, respectively, in excellent agreement with the fitted values, −62.14 and −1.36 cm^{-1}. The comparison between the two Fe_5 complexes shows that the

dx.doi.org/10.1021/ic3024056 | Inorg. Chem. 2013, 52, 1099−1107

additional chloride bridging ligands in **1** weaken the antiferromagnetic coupling between the Fe^{II} ions of the central triangle. Analysis of the exchange pathways for the J_2 interaction shows significant differences between the two complexes that could explain the change in the nature of the interaction. In the symmetric complex **1**, the Fe···Fe distance is 4.746 Å and the Fe−N−N−Fe torsion angle is 16.8°, while in the previously reported nonsymmetric Fe_5 system,[39] the average values for such structural parameters are 4.492 Å and 10.4°, respectively.

For the nonsymmetric Mn_8 complex **2**, all sets of J values confirm the presence of weak antiferromagnetic interaction in such a system and they lead to an $S = 0$ ground state. The fitted J values (see Table 2 with a fitted $g = 2.014$) are slightly smaller than those obtained with the DFT calculations. As for the Fe_5 complex, the strongest antiferromagnetic interaction corresponds to the couplings inside the triangles, in this case through a single μ_3-Cl bridging ligand. However, it is worth remarking that the exchange interaction through both μ_3-O and μ-Cl bridging ligands of complex **1** provides much stronger antiferromagnetic coupling than the single μ_3-Cl bridging ligand of **2**. The three interactions through a double μ-N_2 (triazole) between Mn^{II} ions of different triangles (J_3) are stronger than that with only one μ-N_2 (triazole) single bridging ligand, which corresponds to the interaction between a Mn^{II} cation of the triangle and external Mn^{II} centers (J_2). For the J_2 interactions, the average Mn···Mn distance is 4.62 Å and the Mn−N−N−Mn torsion angle is 10.9°, intermediate values in comparison with the two studied Fe_5 complexes.

CONCLUSIONS

In this study, we reported the successful construction of novel triple-stranded cluster helicates templated by a $[M^{II}_3(\mu_3\text{-O/X})]^{n+}$ triangle core. Two possible self-assembled products, pentanuclear mesocate and octanuclear helicate, could be selectively stabilized by employing the triangle core of different sizes; namely, the smaller core tends to induce the formation of a mesocate, while the one with bigger size results in a helicate structure. Magnetic susceptibility measurements and DFT calculations were performed for complexes **1** and **2**, which revealed an overall intracluster antiferromagnetic coupling. We believe that such a synthetic strategy could be exploited to design more intriguing cluster helicates and mesocates with novel properties.

ASSOCIATED CONTENT

Supporting Information

ESI-MS spectra of **1**, structural diagram showing distorted ligands in **1**, and field dependence of magnetization for **1** and **2**. This material is available free of charge via the Internet at http://pubs.acs.org.

AUTHOR INFORMATION

Corresponding Author

*E-mail: eliseo.ruiz@qi.ub.es (E.R.), tongml@mail.sysu.edu.cn (M.-L.T).

Notes

The authors declare no competing financial interest.

ACKNOWLEDGMENTS

This work was supported by the "973 Project" (2012CB821704), NSFC (Grants 91122032, 90922009, and 21121061), and SRFDP (20100171110015).

REFERENCES

(1) Lehn, J.-M.; Rigault, A. *Angew. Chem., Int. Ed. Engl.* **1988**, *27*, 1095−1097.
(2) Childs, L. J.; Alcock, N. W.; Hannon, M. J. *Angew. Chem., Int. Ed.* **2002**, *41*, 4244−4247.
(3) Hamacek, J.; Blanc, S.; Elhabiri, M.; Leize, E.; Dorsselaer, A. V.; Piguet, C.; Albrecht-Gary, A.-M. *J. Am. Chem. Soc.* **2003**, *125*, 1541−1550.
(4) Albrecht, M. *Angew. Chem., Int. Ed.* **2005**, *44*, 6448−6451.
(5) Albrecht, M.; Mirtschin, S.; de Groot, M.; Janser, I.; Runsink, J.; Raabe, G.; Kogej, M.; Schalley, C. A.; Fröhlich, R. *J. Am. Chem. Soc.* **2005**, *127*, 10371−10387.
(6) Zeckert, K.; Hamacek, J.; Senegas, J.-M.; Dalla-Favera, N.; Floquet, S.; Bernardinelli, G.; Piguet, C. *Angew. Chem., Int. Ed.* **2005**, *44*, 7954−7958.
(7) Katagiri, H.; Miyagawa, T.; Furusho, Y.; Yashima, E. *Angew. Chem., Int. Ed.* **2006**, *45*, 1741−1744.
(8) Du, M.; Bu, X.-H.; Guo, Y. M.; Ribasc, J.; Diaz, C. *Chem. Commun.* **2002**, 2550−2551.
(9) Albrecht, M. *Chem. Soc. Rev.* **1998**, *27*, 281−288.
(10) Caulder, D. L.; Raymond, K. N. *J. Chem. Soc., Dalton Trans.* **1999**, 1185−1200.
(11) Piguet, C.; Bernardinelli, G.; Hopfgartner, G. *Chem. Rev.* **1997**, *97*, 2005−2062.
(12) Albrecht, M. *Chem. Rev.* **2001**, *101*, 3457−3497.
(13) Piguet, C.; Borkovec, M.; Hamacek, J.; Zeckert, K. *Coord. Chem. Rev.* **2005**, *249*, 705−726.
(14) Hannon, M. J.; Moreno, V.; Prieto, M. J.; Moldrheim, E.; Sletten, E.; Meistermann, I.; Isaac, C. J.; Sanders, K. J.; Rodger, A. *Angew. Chem., Int. Ed.* **2001**, *40*, 879−884.
(15) Cardinali, F.; Mamlouk, H.; Rio, Y.; Armaroli, N.; Nierengarten, J.-F. *Chem. Commun.* **2004**, 1582−1583.
(16) Yeung, C.-T.; Yeung, H.-L.; Tsang, C.-S.; Wong, W.-Y.; Kwong, H.-L. *Chem. Commun.* **2007**, 5203−5205.
(17) Albrecht, M.; Kotila, S. *Angew. Chem., Int. Ed. Engl.* **1995**, *34*, 2134−2137.
(18) Enemark, E. J.; Stack, T. D. P. *Angew. Chem., Int. Ed. Engl.* **1995**, *34*, 996−998.
(19) Meyer, M.; Kersting, B.; Powers, R. E.; Raymond, K. N. *Inorg. Chem.* **1997**, *36*, 5179−5191.
(20) Sun, X.; Johnson, D. W.; Caulder, D. L.; Powers, R. E.; Raymond, K. N.; Wong, E. H. *Angew. Chem., Int. Ed.* **1999**, *38*, 1303−1307.
(21) Albrecht, M. *Chem.—Eur. J.* **2000**, *6*, 3485−3489.
(22) Cai, Y.-P.; Su, C.-Y.; Chen, C.-L.; Li, Y.-M.; Kang, B.-S.; Chan, A. S. C.; Kaim, W. *Inorg. Chem.* **2003**, *42*, 163−168.
(23) Argent, S. P.; Adams, H.; Riis-Johannessen, T.; Jeffery, J. C.; Harding, L. P.; Clegg, W.; Harrington, R. W.; Ward, M. D. *Dalton Trans.* **2006**, 4996−5013.
(24) Dul, M.-C.; Pardo, E.; Lescouëzec, R.; Chamoreau, L.-M.; Villain, F.; Journaux, Y.; Ruiz-García, R.; Cano, J.; Julve, M.; Lloret, F.; Pasán, J.; Ruiz-Pérez, C. *J. Am. Chem. Soc.* **2009**, *131*, 14614−14615.
(25) Cui, F.; Li, S.; Jia, C.; Mathieson, J. S.; Cronin, L.; Yang, X.-J.; Wu, B. *Inorg. Chem.* **2012**, *51*, 179−187.
(26) *Metal Clusters in Chemistry*; Braunstein, P., Oro, L. A., Raithby, P. R., Eds.; Wiley-VCH: Weinheim, Germany, 1999; Vols. *1*−*3*.
(27) Bermejo, M. R.; González-Noya, A. M.; Pedrido, R. M.; Romero, M. J.; Vázquez, M. *Angew. Chem., Int. Ed.* **2005**, *44*, 4182−4187.
(28) Bermejo, M. R.; González-Noya, A. M.; Martínez-Calvo, M.; Pedrido, R.; Romero, M. J.; López, M. V. *Eur. J. Inorg. Chem.* **2008**, 3852−3863.
(29) Bera, M.; Aroms, G.; Wong, W. T.; Ray, D. *Chem. Commun.* **2006**, 671−673.
(30) Baxter, P. N. W.; Lehn, J.-M.; Baum, G.; Fenske, D. *Chem.—Eur. J.* **2000**, *6*, 4510−4517.
(31) Vázquez, M.; Bermejo, M. R.; Licchelli, M.; González-Noya, A. M.; Pedrido, R. M.; Sangregorio, C.; Sorace, L.; García-Deibe, A. M.; Sanmartín, J. *Eur. J. Inorg. Chem.* **2005**, 3479−3490.

(32) Pedrido, R.; López, M. V.; Sorace, L.; González-Noya, A. M.; Cwiklinska, M.; Suárez-Gómez, V.; Zaragoza, G.; Bermejo, M. R. *Chem. Commun.* **2010**, *46*, 4797−4799.
(33) Saalfrank, R. W.; Löw, N.; Trummer, S.; Sheldrick, G. M.; Teichert, M.; Stalke, D. *Eur. J. Inorg. Chem.* **1998**, 559−563.
(34) Yoneda, K.; Adachi, K.; Nishio, K.; Yamasaki, M.; Fuyuhiro, A.; Katada, M.; Kaizaki, S.; Kawata, S. *Angew. Chem., Int. Ed.* **2006**, *45*, 5459−5461.
(35) Hou, J.-Z.; Li, M.; Li, Z.; Zhan, S.-Z.; Huang, X.-C.; Li, D. *Angew. Chem., Int. Ed.* **2008**, *47*, 1711−1714.
(36) Zhu, A.-X.; Zhang, J.-P.; Lin, Y.-Y.; Chen, X.-M. *Inorg. Chem.* **2008**, *47*, 7389−7395.
(37) Ishikawa, R.; Nakano, M.; Fuyuhiro, A.; Takeuchi, T.; Kimura, S.; Kashiwagi, T.; Hagiwara, M.; Kindo, K.; Kaizaki, S.; Kawata, S. *Chem.—Eur. J.* **2010**, *16*, 11139−11144.
(38) Romain, S.; Rich, J.; Sens, C.; Stoll, T.; Benet-Buchholz, J.; Llobet, A.; Rodriguez, M.; Romero, I.; Clérac, R.; Mathonière, C.; Duboc, C.; Deronzier, A.; Collomb, M.-N. *Inorg. Chem.* **2011**, *50*, 8427−8436.
(39) Bao, X.; Leng, J.-D.; Meng, Z.-S.; Lin, Z.-J.; Tong, M.-L.; Nihei, M.; Oshio, H. *Chem.—Eur. J.* **2010**, *16*, 6169−6174.
(40) Piguet, C.; Hopfgartner, G.; Bocquet, B.; Schaad, O.; Williams, A. F. *J. Am. Chem. Soc.* **1994**, *116*, 9092−9102.
(41) Aboshyan-Sorgho, L.; Besnard, C.; Pattison, P.; Kittilstved, K. R.; Aebischer, A.; Bünzli, J.-C. G.; Hauser, A.; Piguet, C. *Angew. Chem., Int. Ed.* **2011**, *50*, 4108−4112.
(42) Aboshyan-Sorgho, L.; Cantuel, M.; Bernardinelli, G.; Piguet, C. *Dalton Trans.* **2012**, 7218−7226.
(43) The crystal structure of **5** could be solved in both *P*3*c*1 and $P\bar{3}c1$ space groups without modifying the overall structure. However, the noncentrosymmetric space group tends to be more appropriate because it gives a much smaller *R* parameter (R1/wR2 [$I > 2\sigma(I)$] = 0.0385/0.1060 for *P*3*c*1 and 0.1102/0.3103 for $P\bar{3}c1$) and a twin factor not equal to 0.5 (0.67313).
(44) Becke, A. D. *J. Chem. Phys.* **1993**, *98*, 5648−5652.
(45) Schaefer, A.; Huber, C.; Ahlrichs, R. *J. Chem. Phys.* **1994**, *100*, 5829−5835.
(46) Frisch, M. J.; Trucks, G. W.; Schlegel, H. B.; Scuseria, G. E.; Robb, M. A.; Cheeseman, J. R.; Scalmani, G.; Barone, V.; Mennucci, B.; Petersson, G. A.; Nakatsuji, H.; Caricato, M.; Li, X.; Hratchian, H. P.; Izmaylov, A. F.; Bloino, J.; Zheng, G.; Sonnenberg, J. L.; Hada, M.; Ehara, M.; Toyota, K.; Fukuda, R.; Hasegawa, J.; Ishida, M.; Nakajima, T.; Honda, Y.; Kitao, O.; Nakai, H.; Vreven, T.; Montgomery, J. A., Jr.; Peralta, J. E.; Ogliaro, F.; Bearpark, M.; Heyd, J. J.; Brothers, E.; Kudin, K. N.; Staroverov, V. N.; Kobayashi, R.; Normand, J.; Raghavachari, K.; Rendell, A.; Burant, J. C.; Iyengar, S. S.; Tomasi, J.; Cossi, M.; Rega, N.; Millam, J. M.; Klene, M.; Knox, J. E.; Cross, J. B.; Bakken, V.; Adamo, C.; Jaramillo, J.; Gomperts, R.; Stratmann, R. E.; Yazyev, O.; Austin, A. J.; Cammi, R.; Pomelli, C.; Ochterski, J. W.; Martin, R. L.; Morokuma, K.; Zakrzewski, V. G.; Voth, G. A.; Salvador, P.; Dannenberg, J. J.; Dapprich, S.; Daniels, A. D.; Farkas, Ö.; Foresman, J. B.; Ortiz, J. V.; Cioslowski, J.; Fox, D. J. *Gaussian 09*, revision A.1; Gaussian Inc.: Wallingford, CT, 2009.
(47) *Jaguar 7.0*; Schrödinger, LLC: New York, 2007.
(48) Ruiz, E.; Alemany, P.; Alvarez, S.; Cano, J. *J. Am. Chem. Soc.* **1997**, *119*, 1297−1303.
(49) Ruiz, E.; Cano, J.; Alvarez, S. *Chem.—Eur. J.* **2005**, *11*, 4767−4771.
(50) Ruiz, E.; Cauchy, T.; Cano, J.; Costa, R.; Tercero, J.; Alvarez, S. *J. Am. Chem. Soc.* **2008**, *130*, 7420−7426.
(51) Ruiz, E. *Struct. Bonding (Berlin)* **2004**, *113*, 71−102.
(52) Ruiz, E.; Alvarez, S.; Cano, J.; Polo, V. *J. Chem. Phys.* **2005**, *123*, 164110(1)−164110(7).